Tertiary and Quaternary Structures of 0.19 α-Amylase Inhibitor from Wheat Kernel Determined by X-ray Analysis at 2.06 Å Resolution[†,‡]

Yutaka Oda,[§] Takateru Matsunaga,[§] Keiichi Fukuyama,*[,§] Toshiyuki Miyazaki,[||] and Toshihisa Morimoto[||]

Department of Biology, Graduate School of Science, Osaka University, Toyonaka, Osaka 560, Japan, and Nisshin Flour Milling Co., Ltd., Koami-cho, Nihonbashi, Chuo-ku, Tokyo 103, Japan

Received June 2, 1997; Revised Manuscript Received August 13, 1997[⊗]

ABSTRACT: The crystal structure of 0.19 α-amylase inhibitor (0.19 AI) from wheat kernel was determined by the multiple-isomorphous replacement method coupled with density modification and noncrystallographic symmetry averaging and then refined by simulated annealing using diffraction data to 2.06 Å resolution (R = 18.7%, free R = 22.3%). The asymmetric unit has four molecules of 0.19 AI, each comprised of 124 amino acid residues. Electron density for residues 1−4 and 69−77 is absent in all subunits, probably because of the intrinsic flexibility of these segments. Each subunit has four major α-helices and one one-turn helix which are arranged in the up-and-down manner, maintaining the favorable packing modes of the α-helices. 0.19 AI, however, has two short antiparallel β-strands. All 10 cysteine residues in 0.19 AI form disulfide bonds (C6−C52, C20−C41, C28−C83, C42−C99, and C54−C115), consistent with the assignments made biochemically for 0.28 AI from wheat kernel and by NMR analysis of the bifunctional α-amylase/trypsin inhibitor from ragi seeds (RBI). The disulfide bond patterns in these AIs are similar to those in the hydrophobic protein from soybean (HPS), which lack only the bond corresponding to C28−C83 in 0.19 AI. Extensive interactions occurred between particular pairs of 0.19 AI subunits, mainly involving hydrophobic residues. Comparisons of the structures of 0.19 AI, RBI, and HPS showed that the arrangements of the major α-helices are similar but the conformations of the remaining residues differ markedly. The present X-ray analysis for 0.19 AI and the NMR analysis for RBI suggest that all the AIs in this family have a common fold. The α-amylase binding site is discussed on the basis of the tertiary and quaternary structures of 0.19 AI together with biochemical and spectroscopic data for AIs.

Protein inhibitors of α-amylase are found widely in prokaryotic and eukaryotic cells and have inhibitory activity on α-amylases, the enzymes responsible for cleavage of α-(1−4) glucoside bonds present in glycogen and starch. A large number of α-amylase inhibitors (AIs)[1] have been isolated from plants and microbial sources, and their extensive biochemical, biophysical, and spectroscopic data have been accumulated. About 30 proteins found in cereal seeds, which include trypsin inhibitors as well as AIs, are known to belong to one family on the basis of the homology of their amino acid sequences (*1, 2*). They are, however, unrelated to the AI from *Streptomyces tendae* and the bifunctional serine protease/α-amylase inhibitor from wheat, whose three-dimensional structures are known (*3*−*5*).

AIs of this family are composed of 120−130 amino acid residues and have similar sequences (*1, 2*). Cysteine residues, in particular, are highly conserved. Typically, AIs have ten cysteine residues which form five disulfide bonds. They are resistant to heat treatment and are stable at extreme pH values (*1*). Circular dichroism analysis has shown that AIs have a high α-helix content (*6*), unlike the α-amylase inhibitor from *S. tendae* and the bifunctional serine protease/α-amylase inhibitor from wheat which are composed mostly of β-strands (*3*−*5*). The AIs of this family are present as a monomer, homodimer, or heterotetramer. Although their physicochemical characteristics and interaction with α-amylases have been studied extensively (*6*−*9*), only limited information is available on the tertiary and quaternary structures of the AIs of this family. To date, only the tertiary structure of the bifunctional α-amylase/trypsin inhibitor from ragi seeds (RBI) has been determined by NMR spectroscopy (*2*).

The AI coded 0.19 according to its gel electrophoretic mobility relative to bromophenol blue is one of the most studied AIs of this family and inhibits α-amylases from human saliva, chick pancreas, the yellow mealworm, and *Bacillus subtilis* (*6, 7, 9, 10*). It has 124 amino acid residues, and its amino acid sequence (*11*) is 26% identical with that of RBI (*12*). The known sequence of 0.19 AI and the gel chromatography results of Silano *et al*. (*7*) and Buonocore *et al*. (*9*) indicate that 0.19 AI is a homodimer. To show the structural basis for the inhibitory mechanism of α-amylase, we determined the three-dimensional structure of 0.19 AI by X-ray crystallographic analysis. The results provide a guide for our study of the structure−function relationships using site-directed mutagenesis and for technological studies such as in diabetes control and nutritional and/or toxicologi-

[†] This work was supported in part by a Grant-in-Aid for Cooperative Research (06305006) from the Ministry of Education, Science, Sports, and Culture, Japan, and by the Sakabe project of TARA (Tsukuba Advanced Research Alliance) of the University of Tsukuba.

[‡] The atomic parameters have been deposited in the Brookhaven Protein Data Bank (code 1HSS).

* To whom correspondence should be addressed. Fax: 81-6-850-5425. E-mail: fukuyama@bio.sci.osaka-u.ac.jp.

[§] Osaka University.

[||] Nisshin Flour Milling Co., Ltd.

[⊗] Abstract published in *Advance ACS Abstracts,* October 1, 1997.

[1] Abbreviations: AI, α-amylase inhibitor; IP, imaging plate; NCS, noncrystallographic symmetry; RBI, bifunctional α-amylase/trypsin inhibitor from seeds of ragi; HPS, hydrophobic protein from soybean; UAc, uranyl acetate; PCMB, *p*-chloromercuribenzoate; rms, root-mean-square.

S0006-2960(97)01307-X CCC: $14.00

cal aspects of foods. We report here the tertiary and quaternary structures of 0.19 AI and compare its tertiary structure with the structures of RBI (*2*) and the hydrophobic protein from soybean (HPS) with unknown function (*13*).

EXPERIMENTAL PROCEDURES

Preparation of Heavy-Atom Derivatives. 0.19 AI was purified from wheat flour by the procedure described by Maeda *et al.* (*11*) and crystallized in the space group $P3_1$ (subsequent analysis determined the correct enantiomer described below) with the following unit cell constants: $a = b = 79.3$ Å and $c = 60.8$ Å (*14*). Although one isomorphous heavy-atom derivative was prepared by soaking the crystal in $HgCl_2$ solution, the electron density map based on its single-isomorphous replacement phases could not be interpreted (*14*). We therefore searched for other heavy-atom derivatives with a procedure similar to that used for the mercury derivative. Diffraction data for each derivative crystal were evaluated using a difference Patterson map. Eventually, two new heavy-atom derivatives useful in phase determination were found.

Data Collection and Processing. Each crystal was sealed in a glass capillary tube. Its X-ray diffraction data were collected at room temperature. For the native, $HgCl_2$-, and PCMB-derivative crystals, intensity data were collected using an R-AXIS IIc or IV instrument and CuKα radiation and then processed and scaled using Rigaku software (*15*). Diffraction data for the UAc and $HgCl_2$ derivatives were collected using synchrotron radiation with a screenless Weissenberg camera for macromolecular crystals (*16*) at the $BL6A_2$ station of the Photon Factory at the National Laboratory for High Energy Physics. The second data set for the $HgCl_2$ derivative was focused on the use of anomalous phase information; therefore, the wavelength was set near the absorption edge of the mercury atom. The radius of the film cassette, which contained a Fuji imaging plate (IP) with a detection area of 40 cm × 20 cm, was 429.7 mm. The diffraction intensities recorded on each IP were read out with Fuji BA100 for the UAc derivative and with BAS2000 for the $HgCl_2$ derivative. They were processed and scaled with the WEIS program (*17*) for the former and with DENZO (*18*) and SCALEPACK (*19*) for the latter. Results of the data collection and some of the experimental conditions are given in Table 1.

Rotation Function. It was most probable that the four 0.19 AI subunits were contained in the asymmetric unit on the basis of the V_m value (*20*) (2.1 Å^3/Da for four subunits) because 0.19 AI exists as a dimer. The $\kappa = 180°$ section of a self-rotation function using the native data is shown Figure 1. There are a major peak (P) at $\psi = 90°$ and $\phi = 3°$ and two minor peaks (Q and R) at $\psi = 37°$ and $\phi = 95°$ and $\psi = 53°$ and $\phi = 275°$, respectively. These three 2-fold axes are perpendicular to each other. This suggests that four subunits of 0.19 AI in an asymmetric unit are associated with satisfying 222 symmetry.

Phase Determination and Improvement. Major heavy-atom sites were located in the difference Patterson maps, and their sites and occupancies were refined with the CCP4 program suite (*21*). The correct space group was determined to be $P3_1$ on the basis of the anomalous scattering data of the $HgCl_2$ derivative (*22*). The minor heavy-atom sites in each derivative were subsequently located by difference

Table 1: Data Collection and Phasing Statistics

	native	$HgCl_2$(1)	$HgCl_2$(2)	UAc	PCMB
concentration (mM)	−	3	3	5	2
soaking time (h)	−	4	10	2	24
wavelength (Å)	1.5418	1.5418	0.995	1.04	1.5418
resolution limit (Å)	2.06	2.06	3.3	2.4	3.5
measured reflections	49 815	62 783	18 574	20 510	18 331
independent reflections	22 687	22 834	5 906	11 154	5 347
completeness (%)[a]	81.9 (67.3)	83.0 (70.0)	85.0 (73.2)	66.7 (51.0)	88.8 (92.6)
R_{merge} (%)[a,b]	5.7 (15.0)	5.5 (24.0)	2.6 (3.3)	4.8 (8.4)	7.1 (7.0)
R_{iso} (%)[c]		12.2	20.8	24.6	11.2
R_{ano} (%)[d]		−	4.3	−	−
no. of heavy-atom sites		8	12	7	9
resolution for phasing (Å)		15.0−3.0	15.0−3.3	15.0−3.0	15.0−3.5
R_{Cullis}(iso)[e]		0.74	−	0.77	0.95
R_{Cullis}(ano)[f]		−	0.98	−	−
phasing power		1.48		1.32	0.52

[a] Numerals in parentheses are for the data in the highest-resolution shell. [b] $R_{merge} = \Sigma_h\Sigma_i|I_i(hkl)-\langle I(hkl)\rangle|/\Sigma_h\Sigma_i\langle I(hkl)\rangle$. [c] $R_{iso} = \Sigma|I_{PH}(hkl)-I_P(hkl)|/\Sigma|I_P(hkl)|$. [d] $R_{ano} = \Sigma|I_{PH}(hkl)-I_{PH}(-h-k-l)|/\Sigma|I_{PH}(hkl)|$. [e] $R_{Cullis}(iso) = \Sigma||\mathbf{F}_{PH} - \mathbf{F}_P|-\mathbf{F}_H|/\Sigma|F_{PH}-F_P|$. [f] $R_{Cullis}(ano) = \Sigma||F_{PH}(hkl)-F_{PH}(-h-k-l)|-2F_H''\sin(\alpha_{PH}-\alpha_H)|/\Sigma|F_{PH}(hkl)-F_{PH}(-h-k-l)|$.

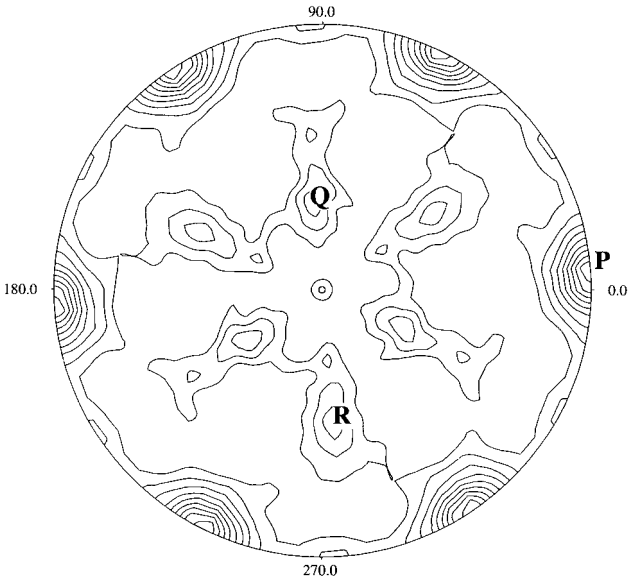

FIGURE 1: Self-rotation function of the 0.19 AI native crystal at the $\kappa = 180°$ section calculated with POLARRFN. Data in the range of 15.0−2.5 Å were used. The radius of integration is 15 Å.

Fourier syntheses using the phases derived from multiple-isomorphous replacement and anomalous scattering methods. The phase angles and figures of merit were calculated with MLPHARE (*23*). The overall figure of merit was 0.495 for 8345 reflections between 15 and 3.0 Å resolution. The phasing results are shown in Table 1. The quality of the electron density map was not sufficient to be able to identify the boundary of each subunit or to trace any of the polypeptide chains. Although we expected that the heavy atoms would bind to equivalent sites in each subunit, we were unable to locate the local symmetries from the heavy-

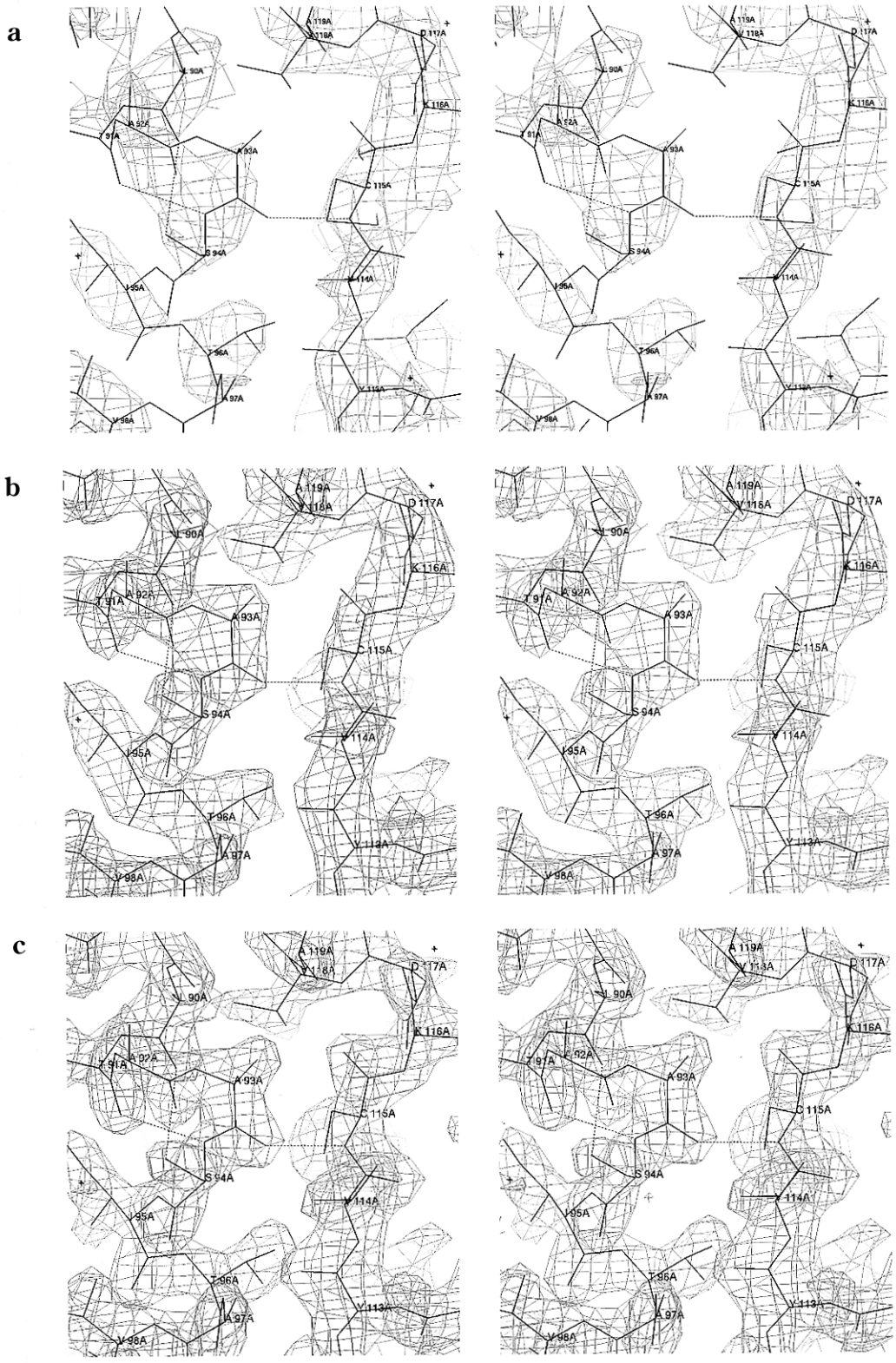

FIGURE 2: Electron densities (contoured at 1.5σ) at three different stages of the analysis superimposed on the final model: (a) the density calculated with phases by multiple-isomorphous replacement and anomalous scattering methods at 3.0 Å resolution, (b) the density after averaging by NCS at 2.6 Å resolution, and (c) the final $2F_o - F_c$ at 2.06 Å resolution. At the center of the figure Ser94 is located, where α4 is bent. The hydrogen bonds between the pairs of atoms that are nonstandard for the α-helix are shown by dotted lines. The distances are as follows: C115N···A93O, 2.8 Å; S94N···T91O, 3.1 Å; and S94O_γ···L90O, 3.1 Å.

atom sites even in reference to their orientations derived from the rotation function.

The phase angles were improved by density modification using the program DM (*24*) which includes solvent flattening and histogram matching. Careful inspection of the resulting electron density map revealed several α-helices and similar features that may belong to different subunits. With their arrangements as a guide, the transformations that relate the subunits were eventually determined. Three local symmetry operators gave significant correlations between related electron density regions and are consistent with the results of the rotation function.[2] Use of noncrystallographic sym-

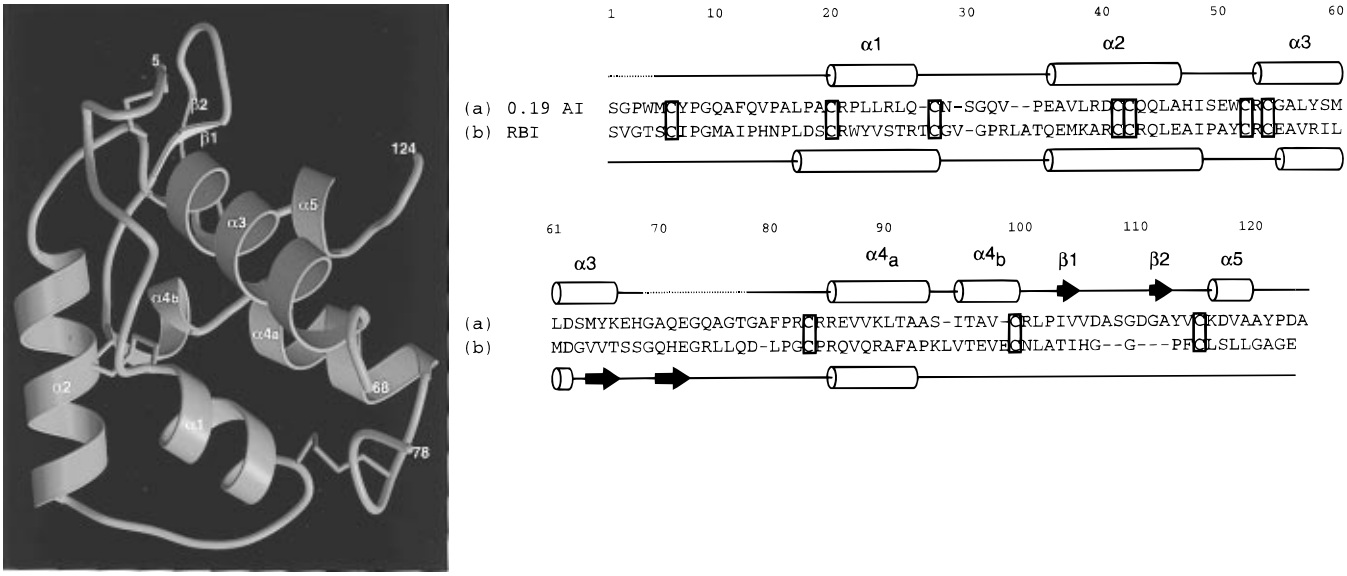

FIGURE 3: Structure of 0.19 AI. (a, left) Schematic drawing of the 0.19 AI subunit drawn by MOLSCRIPT (*29*) and RASTER3D (*30*). Residues 1−4 and 69−77 are absent. The five disulfide bonds are shown in orange. (b, right) Secondary structure assignments and sequence alignment of 0.19 AI (*11*) and RBI (*12*).

metry (NCS) averaging for the four subunits and density modification greatly improved the overall figure of merit to 0.712 and produced an electron density map that could be interpreted (Figure 2).

Model Building and Crystallographic Refinement. The map allowed the tracing of the major portion of the polypeptide chain. A model was built for one of the four subunits using TURBO-FRODO (*26*) and SGI Indigo[2] XZ with the aid of the amino acid sequence (*11*). The model was fitted in the electron density for 107 of 124 residues, but the electron density for both the terminal residues and loop region between α3 and α4 was too poor to build a model. The coordinates of this subunit were expanded by NCS to yield those of the other three subunits.

The structure was refined by alternate cycles of simulated annealing using the program XPLOR (*27*) and manual revision of the model. Initial refinement using the diffraction data between 10 and 2.4 Å resolution (15 440 reflections with an F of $>2\sigma_F$ as the work set, 91% of the available data) reduced the crystallographic R and free R factors to 22.2 and 26.9%, respectively. NCS restraints were applied throughout the refinement. A $2F_o - F_c$ map was used to build the model of the residues not included in the previous cycle of refinement due to conformational uncertainty, as well as to revise the model already built. Peaks in the $F_o - F_c$ map greater than 2.5 times the standard deviation of the map were identified as water molecules. Including water molecules whose occupancy was fixed at 1.0, refinement was continued using the diffraction data to 2.06 Å. Results of crystallographic refinement are shown in Table 2.

RESULTS AND DISCUSSION

Quality of the Model. The current model of 0.19 AI includes 444 residues from four subunits and 264 water molecules per asymmetric unit. In each subunit, both the main and side chains were located for residues 5−68 and 78−124. The electron densities for residues 1−4 and 69−77 were too weak to build a model. These residues appear to be disordered. All the residues modeled fall within the allowed conformation region of a Ramachandran plot (Table 2).

Table 2: Results of Crystallographic Refinement

resolution range (Å)	10.0−2.06
number of reflections used ($F > 2\sigma_F$)	20 451
number of atoms refined[a]	3624 (264)
crystallographic and free R factors (%)	18.7 and 22.3
average B factor for protein atoms (Å^2)	30.6
rms deviations from ideal geometry	
bonds (Å)	0.012
angles (deg)	1.4
NCS mean deviations among four subunits	
coordinates (Å)	0.10−0.14
B factors (Å^2)	3.4−6.6
Ramachandran plot[b]	
residues in core regions (%)	89.4
residues in allowed regions (%)	10.6

[a] The numeral in parentheses is for water molecules. [b] PROCHECK (*28*).

Tertiary Structure of the Subunit. The present crystallographic analysis established the fact that the asymmetric unit has four subunits (A−D). The secondary structures of each subunit are identical. We describe first the tertiary structure of the A subunit. A schematic drawing of this subunit and the secondary structure assignment of 0.19 AI are shown in Figure 3.

As shown by CD spectroscopy for 0.19 AI (*6*) and NMR analysis for RBI (*2*), 0.19 AI has a high α-helix content. 0.19 AI has five α-helices (α1−α5), although α4 is bent at Ser94 (Figure 2). Only Ser94 in the segment from residues 85 to 99 deviates from the conformation of the α-helix ($\phi = -117 \pm 1°$ and $\psi = 16 \pm 1°$), causing the bending of α4 and disruption of the hydrogen bonds between the carbonyl groups of Leu90−Ala93 and the amide groups of Ser94−Ala97. Instead, the side chain of Ser94 participates in hydrogen bonding with the main chain carbonyl group of

[2] After our crystallization of 0.19 AI was published (*14*), Oliva *et al.* obtained crystals of this AI under different conditions, but their crystals had the same space group as ours and the identical unit cell dimensions (*25*). They suggested the presence of a local 222 symmetry based on the self-rotation function. Our present crystallographic analysis confirmed its presence in the 0.19 AI crystal, but the directions of two of the three 2-fold axes (Q and R axes) that they assigned are not correct.

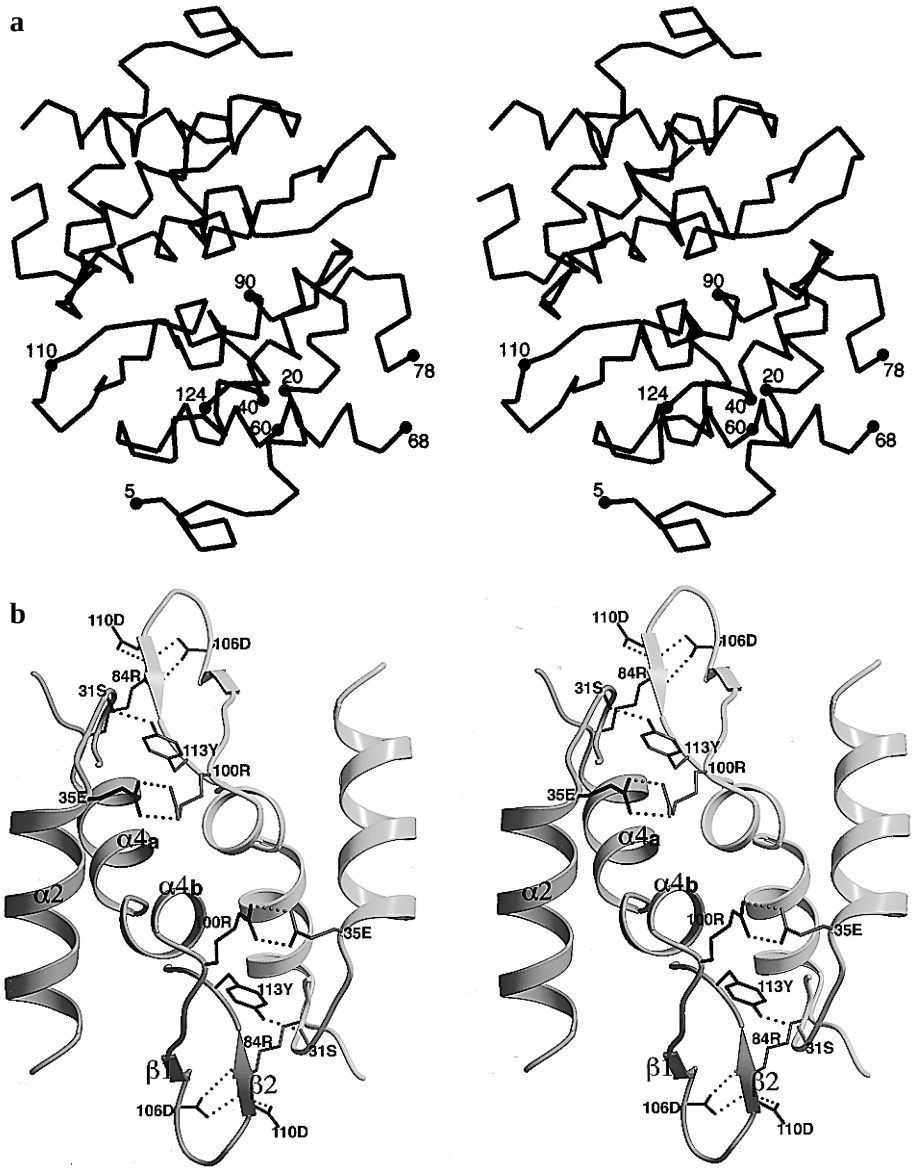

FIGURE 4: Stereoviews of (a) a C_α tracing of the 0.19 AI dimer (A and B subunits) and (b) a closeup view of the dimer interface viewed along the noncrystallographic 2-fold axis: dark, A subunit; and light, B subunit. The average interatomic distances by NCS are as follows: S31O···Y113O$_\eta$, 2.7 Å; E35O$_{\epsilon1}$···R100N$_{\eta2}$, 2.7 Å; E35O$_{\epsilon2}$···R100N$_{\eta1}$, 2.9 Å; R84N$_{\eta1}$···D106O$_{\delta1}$, 2.8 Å; R84N$_{\eta2}$···D106O$_{\delta2}$, 3.1 Å; and R84N$_{\eta2}$···D110O$_{\delta2}$, 3.0 Å.

Leu90 (Figure 2). Two segments, 103 and 104 and 111 and 112, form short antiparallel β-strands (β1 and β2).

The five helices in 0.19 AI are arranged in an up-and-down manner, satisfying the favorable packing modes of α-helices. The intersecting angle of the helix axes of α1−α2 is 48°. This is a representative helix−helix interaction seen in globins (*31*). The three helices of α3−α5 form angles similar to those in four-helix bundle proteins, the angles of α3−α4, α3−α5, and α4−α5 being 30, 14, and 16°, respectively. These are in the range required for the favorable packing of antiparallel α-helices.

All 10 cysteine residues in 0.19 AI form disulfide bonds which occur in the pairs Cys6−Cys52, Cys20−Cys41, Cys28−Cys83, Cys42−Cys99, and Cys54−Cys115. The pattern of the disulfide bonds in 0.19 AI is identical with the patterns in 0.28 AI (*32*) and in RBI (*2*). All χ^3 values (torsion angle of $C_\beta-S_\gamma-S_\gamma-C_\beta$) are close to 90 or −90°, whereas most χ^2 values (torsion angle of $C_\alpha-C_\beta-S_\gamma-S_\gamma$) deviate significantly from 90 or −90°.

Quaternary Structure. 0.19 AI is reported to exist as a dimer in solution (*7*, *9*). Of the several kinds of subunit−subunit interactions observed in the present crystal form, the most extensive interactions are in the A−B and C−D subunit pairs. (The C−D subunit pair is related to the A−B subunit pair by NCS.) The sets of interactions in these pairs are equivalent for all four subunits, and we concluded that the A−B and C−D pairs correspond to the dimer of 0.19 AI in solution. The arrangement of the A and B subunits is shown in Figure 4a.

As shown in Figure 4b, the interface between the A and B subunits (between the C and D subunits as well) is mainly composed of α4, the C-terminal loop (Asp110−Lys116), and the turn (Asn29−Glu35) connecting α1 and α2. These segments form a relatively flat surface. It is noteworthy that most residues that make up the interface of the subunits are hydrophobic (see Figure 5). α4, which is located in the middle of the surface, is composed mostly of hydrophobic residues. In addition, the side chain of Ser94 in α4 is not

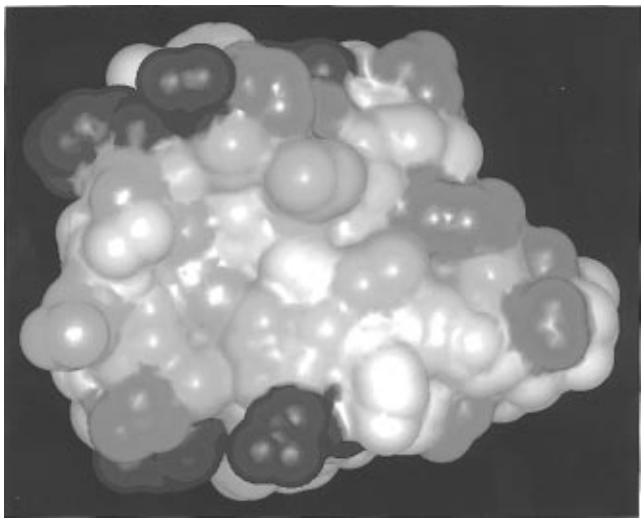

FIGURE 5: Hydrophobicity of the proposed interface of the dimer. α4 is from upper-left to lower-right of the front surface: red, hydrophobic; and blue, hydrophilic. The figure was drawn with Insight II (Biosym/MSI).

exposed outward because it participates in hydrogen bonding with the main chain carbonyl group of Leu90 (Figure 2).

Several water molecules are present in the small cavities of the interface. There are five water molecules in the cavity formed by α4 and the C-terminal loop in the A subunit and α4 and the turn connecting α1 and α2 in the B subunit. Because there is a noncrystallographic 2-fold axis in the middle of the interface, five water molecules are arranged in the cavity on the other side of the interface in a similar manner. Only one water molecule in each cavity, however, connects the A and B subunits. Therefore, it appears that hydrophobic interaction functions mainly to maintain the dimer.

Additional interactions between subunits involve α1 of the B and C subunits, but they appear to be less substantial. The interface between the B and C subunits is more hydrophilic than that between subunits of the putative dimer. No combination of subunit pairs in the unit cell has more extensive subunit−subunit interaction than that described above. These observations also support the fact that the A−B and C−D pairs correspond to the dimer of 0.19 AI.

Heavy-Atom Binding Sites. When the 0.19 AI crystals were soaked in the buffer containing $HgCl_2$, mercury bound to only one major site per asymmetric unit even though four protein subunits are present. The environment of the major mercury site is shown in Figure 6. It is in a shallow hydrophilic pocket near the surface of the C subunit. The mercury is coordinated by Gln44O, His47$N_{\delta 1}$, and Gln13$O_{\epsilon 1}$ of the C subunit. The $F_{Hg} - F_p$ difference Fourier map showed no significant electron density in the corresponding sites of the other three subunits. The minor mercury sites are unrelated to this major site.

Superpositioning the four subunits has shown that the side chain of His47 of the C subunit deviates significantly from the side chains of the other subunits. The locations and conformations of the other residues around this site are essentially identical among the four subunits. The side chain of Trp51 of the other subunit (B subunit operated by crystallographic symmetry) is near the imidazole ring of the His47 of the C subunit. Apparently, the indole ring displaced the imidazole ring toward Gln13$O_{\epsilon 1}$ to form a pocket suitable for mercury ion binding. Around the histidines of the other three subunits, no residues are in close contact with them.

Comparison of the Structures of 0.19 AI and RBI. Sequence alignment showed that 0.19 AI and RBI are members of an inhibitor family, comprised of more than 20 inhibitors found in cereal seeds (*1*, *2*). The three-dimensional structure of RBI, which is 26% identical with 0.19 AI, has been studied in solution using multidimensional ^1H and ^{15}N NMR spectroscopy (*2*). The superposition of the A subunit of 0.19 AI on RBI is shown in Figure 7a. Relative to RBI, two short helices (α4b and α5) also are found in 0.19 AI; α4b follows α4a, and α5 is in the C-terminal region. Although the major α-helices (α1−α4) of 0.19 AI can be superimposed relatively well on those of RBI (rms deviation

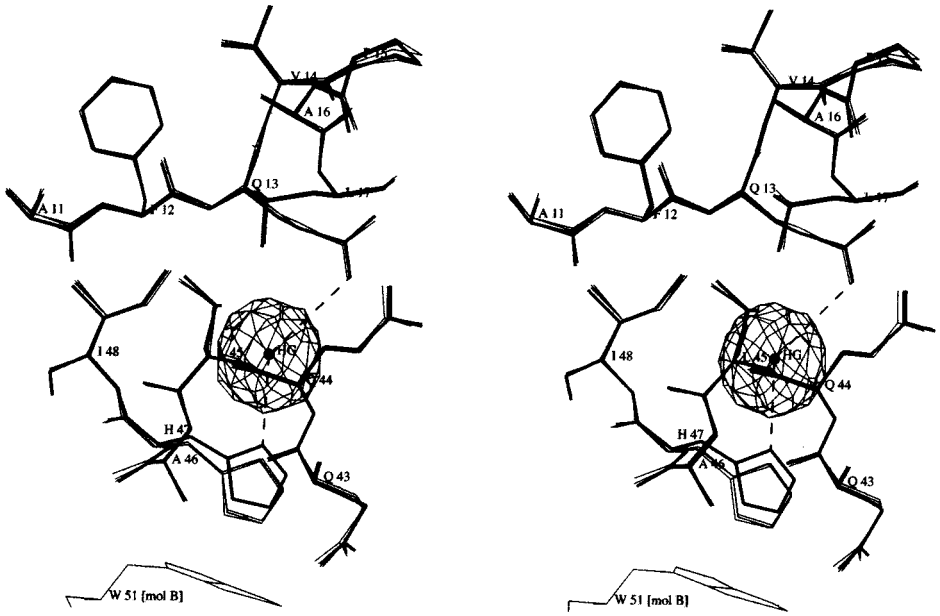

FIGURE 6: Environment of the major mercury site shown by a stereopair. Electron density of the $F_{Hg} - F_p$ difference Fourier map contoured at 5σ is superimposed on the final models of the four subunits (thick bonds, C subunit; and thin bonds, A, B, and D subunits). The phase angles after NCS averaging were used. The distances to the mercury ion are as follows: His47$N_{\delta 1}$, 3.1 Å; and Gln13$O_{\epsilon 1}$, 3.1 Å. The distance between the $C_{\delta 2}$ atom of His47 and the plane of the indole ring of Trp51 is 2.9 Å.

FIGURE 7: Superpositions of (a) 0.19 AI (thick bonds) and RBI (thin bonds) and (b) 0.19 AI (thick bonds) and HPS (thin bonds). Residue numbers of 0.19 AI are underlined. In each pair, the two protein structures were superimposed using the program MFIT (Y. Matsuura, unpublished) to minimize the rms deviation of the corresponding main chain atoms.

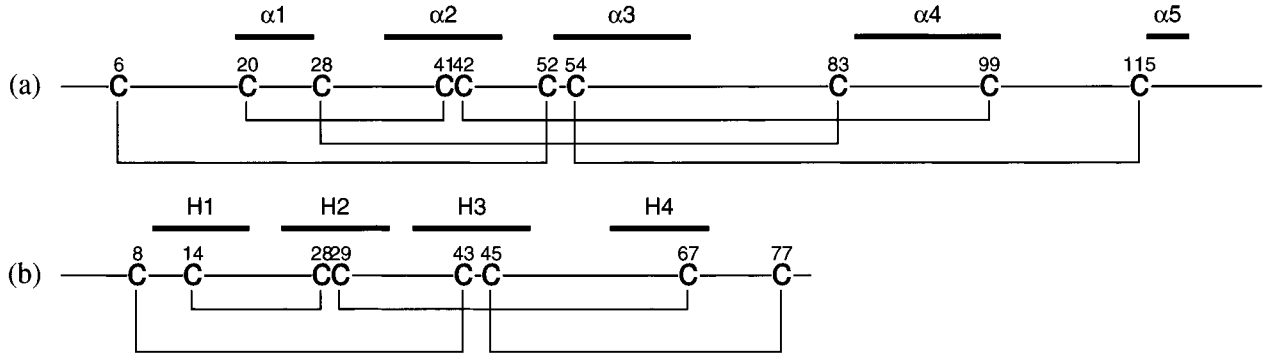

FIGURE 8: Schematic representation of the disulfide bond patterns in (a) 0.19 AI and (b) HPS. Above the representations are the regions of the α-helices. For the sake of clarity, α4a and α4b in 0.19 AI are shown together as α4.

of the main chain atoms for 37 residues is 1.4 Å), the conformations of the remaining residues differ markedly. In particular, the characteristic protruding segment in RBI, which includes antiparallel β-strands between α3 and α4, is absent in 0.19 AI. Most residues that correspond to this segment in 0.19 AI are disordered. Instead, the characteristic protruding segment that includes short antiparallel β-strands is present on the other side of 0.19 AI, where the C-terminal segment is positioned in RBI. In 0.19 AI, the C-terminal segment extends on the backside of the molecule, as shown in Figure 7a. A comparison of the two structures suggests that all the AIs in this family have a basic common fold but that the conformations of their loop regions are divergent.

Although residues 5−68 and 78−124 of 0.19 AI are well-defined and have substantially identical conformations for the four subunits, the electron density for residues 1−4 and 69−77 is absent in all four subunits. This implies that residues 1−4 and 69−77 of 0.19 AI have multiple conformational states. In RBI, the segment corresponding to residues 69−77 in 0.19 AI forms a loop that has short antiparallel β-strands. The difference between 0.19 AI and RBI is probably due to the different features of the two molecules rather than to the different techniques used or differences in the molecular environments (crystal versus solution).

Comparison of the Structures of AIs and HPS. The automated method for comparing protein structures developed by Holm and Sander (*33*) found that, of the proteins deposited in the Brookhaven Protein Data Bank, a 8.3 kDa hydrophobic protein from soybean (HPS), whose function

is unknown (*13*), is significantly structurally similar to 0.19 AI. Although the four α-helices of HPS can be superimposed on those of 0.19 AI with an rms deviation of the main chain atoms for 34 residues of 1.2 Å, the lengths and conformations of the segments connecting the α-helices differ considerably (Figure 7b). (In the 0.19 AI−HPS pair, the fourth helix in HPS can be superimposed on α4b better than α4a in 0.19 AI.) HPS consists of 80 residues, shorter by 44 residues than 0.19 AI. This shortening is primarily compensated for by a more direct connection between α3 and α4.

The similarity in the patterns of the disulfide bonds in AIs and in HPS is clear in Figure 8. HPS has eight cysteine residues with the distribution ...C...C...CC...CXC...C...C... that form four disulfide bonds. The cysteine residues corresponding to the 28th and 83rd cysteine residues in 0.19 AI are replaced by other residues in HPS. Aside from the absence of a disulfide bond corresponding to C28−C83 in 0.19 AI, the patterns of bonds are identical. Although AIs and HPS have similar distributions of the cysteine residues, there is scarcely any homology between their amino acid sequences.

It should be noted that the positions of the disulfide bonds in the tertiary structures are not necessarily conserved. For example, although the consecutive cysteine residues (C41 and C42 in 0.19 AI and C28 and C29 in HPS) are both located in the second α-helices, C52 and C54 in 0.19 AI (the characteristic sequence of cysteine residues CXC) are located before and at the beginning of α3, whereas C43 and C45 in HPS are at the middle of H3.

α-*Amylase Binding Site in 0.19 AI*. Strobl *et al*. reported that the trypsin binding loop of RBI takes the canonical conformation observed in many other serine protease inhibitors (*2*). The corresponding region (the loop between α1 and α2) in 0.19 AI is much shorter than that in RBI (Figure 7a) and, unlike that in RBI, has neither an arginine nor a lysine residue. These findings are consistent with the finding that 0.19 AI has no inhibitory effect on proteases (*34*).

Although 0.19 AI and the α-amylases from the yellow mealworm (*Tenebrio molitor* L. Larva) and chicken pancreas are reported to form 1:1 complexes with respective dissociation constants of 0.85 and 3.7 nM (*8*, *9*), little is known about the α-amylase binding site. Various interpretations of the α-amylase binding site have been proposed on the basis of biochemical and spectroscopic data due to limited information about its three-dimensional structure. For example, involvement of tryptophan and tyrosine residues has been suggested in the binding of α-amylase and RBI (*35*), whereas chemical modification experiments indicate that Lys96 in RBI may be involved in binding to mammalian α-amylase (*36*).

Alagiri and Singh (*35*) and Maskos *et al*. (*37*) showed that α-amylase and trypsin bind independently to RBI. Strobl *et al*. therefore supported the idea of Lys96 in RBI as an α-amylase binding site because the C_α of Lys96 is separated by 23 Å from the C_α of Arg34 in the trypsin binding loop (*2*). The Lys96 in RBI corresponds to the Ser94 in 0.19 AI that is located in α4. When the dimer of 0.19 AI is formed, as shown in Figure 4, this residue is buried inside it. Therefore, the region that includes Ser94 is an unlikely candidate for the α-amylase binding site. Assignment of the Lys96 in RBI to the binding site was based on the fact that modification of the amino groups of RBI with 2,4,6-trinitrobenzenesulforic acid resulted in the loss of α-amylase-inhibitory activity (*36*). Other interpretations of this result, however, are possible; e.g., modification of the amino group of the first residue caused a loss of activity.

Although the tryptophan and tyrosine residues in RBI are reported to be involved in the α-amylase binding site (*35*), these residues are not conserved in the other AIs, including 0.19 AI. In addition, they are involved in the stabilization of the trypsin binding loop in RBI (*2*). At present, there is definitive evidence neither for the α-amylase binding site nor for the inhibitory mechanism of the AIs. Further experiments, such as three-dimensional structural analysis of the α-amylase−AI complex and site-directed mutagenesis of the AIs of this family, are required.

ACKNOWLEDGMENT

We thank Professor Noriyoshi Sakabe of the University of Tsukuba and Drs. Nobuhisa Watanabe and Mamoru Suzuki of the National Laboratory for High Energy Physics for their aid in the data collection with the Weissenberg camera; the staff of the Research Center for Protein Engineering (Institute for Protein Research, Osaka University) for the use of the R-AXIS IIc instrument; and Dr. Genji Kurisu for his help in preparing Figure 5. A part of this research was done with the approval of the Photon Factory Advisory Committee (Proposal 94G042).

REFERENCES

1. Buonocore, V., and Silano, V. (1986) in *Advances in Experimental Medicine and Biology* (Friedman, M., Ed.) Vol. 199, pp 483−507, Plenum Press, New York.
2. Strobl, S., Mühlhahn, P., Bernstein, R., Wiltscheck, R., Maskos, K., Wunderlich, M., Huber, R., Glockshuber, R., and Holak, T. A. (1995) *Biochemistry 34*, 8281−8293.
3. Pflugrath, J. W., Wiegand, G., Huber, R., and Vértesy, L. (1986) *J. Mol. Biol. 189*, 383−386.
4. Zemke, K. J., Müller-Fahrnow, A., Jany, K., Pal, G. P., and Saenger, W. (1991) *FEBS Lett. 279*, 240−242.
5. Kline, A. D., Braun, W., and Würthrich. K. (1986) *J. Mol. Biol. 189*, 377−382.
6. Petrucci, T., Rab, A., Tomasi, M., and Silano, V. (1976) *Biochim. Biophys. Acta 420*, 288−297.
7. Silano, V., Pocchiari, F., and Kasarda, D. D. (1973) *Biochim. Biophys. Acta 317*, 139−148.
8. Buonocore, V., Gramenzi, F., Pace, W., Petrucci, T., Poerio, E., and Silano, V. (1980) *Biochem. J. 187*, 637−645.
9. Buonocore, V., Giardina, P., Parlamenti, R., Poerio, E., and Silano, V. (1984) *J. Sci. Food Agric. 35*, 225−232.
10. Takase, K. (1994) *Biochemistry 33*, 7925−7930.
11. Maeda, K., Wakabayashi, S., and Matsubara, H. (1985) *Biochim. Biophys. Acta 828*, 213−221.
12. Campos, F. A. P., and Richardson, M. (1983) *FEBS Lett. 152*, 300−304.
13. Baud, F., Pebay-Peyroula, E., Cohen-Addad, C., Odani, S., and Lehmann, M. S. (1993) *J. Mol. Biol. 231*, 877−887.
14. Miyazaki, T., Morimoto, T., Fukuyama, K., and Matsubara, H. (1994) *J. Biochem. 115*, 179−181.
15. Higashi, T. (1990) *PROCESS: A Program for Indexing and Processing R-AXIS II Imaging Plate Data*, Rigaku Corp., Tokyo.
16. Sakabe, N. (1991) *Nucl. Instrum. Methods Phys. Res., Sect. A 303*, 448−463.
17. Higashi, T. (1989) *J. Appl. Crystallogr. 22*, 9−18.
18. Otwinowski, Z. (1993) *DENZO: an oscillation data processing program for macromolecular crystallography*, Yale University Press, New Haven, CT.
19. Otwinowski, Z. (1993) *SCALEPACK: software for the scaling together of integrated intensities measured on a number of*

separate diffraction images, Yale University Press, New Haven, CT.
20. Matthews, B. W. (1968) *J. Mol. Biol. 33*, 491−497.
21. Collaborative Computational Project, Number 4 (1994) *Acta Crystallogr. D 50*, 760−763.
22. Strahs, G., and Kraut, J. (1968) *J. Mol. Biol. 35*, 503−512.
23. Otwinowski, Z. (1991) MLPHARE: Maximum likelihood of heavy atom parameters, in *Proceedings of the CCP4 Study Weekend* (Wolf, W., Evans, P. R., and Leslie, A. G. W., Eds.) pp 80−86, SERC Daresbury Laboratory, Warrington, U.K.
24. Cowtan, K. D., and Main, P. (1996) *Acta Crystallogr. D 52*, 756−764.
25. Oliva, G., Iulek, J., and Ida, E. I. (1996) *Acta Crystallogr. D 52*, 1016−1017.
26. Roussel, A., and Cambillau, C. (1989) in *Silicon Graphics Geometry Partner Directory*, pp 77−78, Silicon Graphics, Mountain View, CA.
27. Brünger, A. T. (1992) *XPLOR Version 3.0: A System for X-ray Crystallography and NMR*, Yale University Press, New Haven, CT.
28. Laskowski, R. A., MacArthur, M. W., Moss, D. S., and Thronton, J. M. (1993) PROCHECK: a program to check the stereochemical quality of protein structures, *J. Appl. Crystallogr. 26*, 283−291.
29. Kraulis, P. J. (1991) MOLSCRIPT: a program to produce both detailed and schematic structures, *J. Appl. Crystallogr. 24*, 946−950.
30. Merritt, E. A., and Murphy, M. E. P. (1994) *Acta Crystallogr. D 50*, 869−873.
31. Chothia, C., Levitt, M., and Richardson, D. (1981) *J. Mol. Biol. 145*, 215−250.
32. Poerio, E., Caporale, C., Carrano, L., Pucci, P., and Buonocore, V. (1991) *Eur. J. Biochem. 199*, 595−600.
33. Holm, L., and Sander, C. (1993) *J. Mol. Biol. 233*, 123−138.
34. Choudhury, A., Maeda, K., Murayama, R., and DiMagno, E. P. (1996) *Gastroenterology 111*, 1313−1320.
35. Alagiri, S., and Singh, T. P. (1993) *Biochim. Biophys. Acta 1203*, 77−84.
36. Shivaraj, B., and Pattabiraman, T. N. (1981) *Biochem. J. 193*, 29−36.
37. Maskos, K., Huber-Wunderlich, M., and Glockshuber, R. (1996) *FEBS Lett. 397*, 11−16.

BI971307M